ILASS–Europe 2017, 28th Conference on Liquid Atomization and Spray Systems, 6-8 September 2017, Valencia, Spain
http://dx.doi.org/10.4995/ILASS2017.2017.4987

Large eddy simulations of atomisation and sprays: application to a high pressure multihole injector

Chausserie-Laprée Paul[1], Hélie Jérome[1*], Chesnel Jeremy[2], Demoulin Francois-Xavier[3]
[1]Continental Automotive, Toulouse, France,
[2]ALTRAN, Toulouse, France
[3]CORIA, Rouen, France, demoulin@coria.fr
*Corresponding author: jerome.helie@continental-corporation.com

Abstract
A weak coupling strategy is proposed to simulate the pressurised spray without any empirical readjustment. Volume Of Fluid is used to simulate the nozzle internal flow with cavitation and its primary atomization into ligaments. Lagrangian simulations are then used to get the spray evolution, even temporal. Large Eddy Simulations are used for these two simulations types. The coupling between both is realized by a recording and an analysis of the ligaments with local break up modelling into drops. Two test cases are presented, the second one deals with full, complex geometry, 6-holes Gasoline Direct Injection nozzle. Such approach shows a huge potential for prediction of the final spray from the nozzle geometry.

Keywords
Large Eddy Simulation, spray, multihole, atomization, Volume Of fluid

Introduction
The present work is driven within the industrial automotive contextual aim of reducing the carbon particles emission of car engines. It has been shown that these emissions can be linked to the liquid wall films generated by the penetration of gasoline sprays (i.e. drop jets generated by pressurized atomizer, without assistance of a coflow) impacting on the engine walls. Therefore a better understanding of these sprays physics through simulations is needed. To do so, we developed an Euler-Lagrange solver, implemented in the OpenFOAM platform which allows us to model the non-evaporating gasoline sprays from high-pressure injectors: Large Eddy Simulation (LES) is used for the carrier phase whereas Lagrangian simulation is used for the dispersed phase. A 2-way coupling between the 2 phases and several subgrid submodels have been investigated [1]. The Lagrangian simulation uses the treated results of a Large Eddy-Volume Of Fluid simulation of the cavitating and atomizing flow within and at the close exit of the nozzle. This strategy is efficient because at least one order of magnitude separates the characteristic times of each type of flow but request an effort in the coupling which is specifically described in the present paper.

Simulation Approach
Second order numerical schemes are used for spatial and temporal discretisations. The numerical developments are based on OpenFoam® platform. For the Volume OF Fluid (VOF) approach, first-order reconstruction of the interface is used together with the sharpening process of Weller, see for instance [2]. The subgrid models used in this work are the one-equation eddy for the LES-VOF and the dynamic Smagorinski for the lagrangian-LES,. The choice of the first one is due to the presence of walls and flow detachment inside the nozzle, and the choice of the second one is due to the capture of transitional turbulent jet flow that requires a minimum of numerical dissipation. For more details on the lagrangian simulations, the readers are referred to Helie et al. [1].
To carry out the lagrangian computation of the drops, a special attention is required for the spray inlet condition. This is done through an original weak coupling with LES-VOF simulation of the flow in the internal part and close-vicinity of the nozzle (see for instance [3]). The liquid instantaneous presence and the associated velocity field are stored to be reused identically as input of the spray. The primary atomization process is then analysed and a modelling approach is proposed in 2 steps: Firstly, a rupture into ligaments, almost bidimensional, and a second step where these ligaments propagate further and atomise into rounded ligaments and then into drop populations. Figure 1 left indicates the sketch of this process for one single ligament, the flow being a set of numerous different ligaments. This paradigm of considering a set of different ligaments that will be individually modeled is, to our knowledge, new. The first step is captured with a limited computational effort in the LES-VOF simulation, whereas the second step will be approached using well-established sheet atomization models from the literature. The first

EDITORIAL UNIVERSITAT POLITÈCNICA DE VALÈNCIA

step from the LES-VOF results gives the ligament structures at each instant, and the atomization model returns the final drop size population.

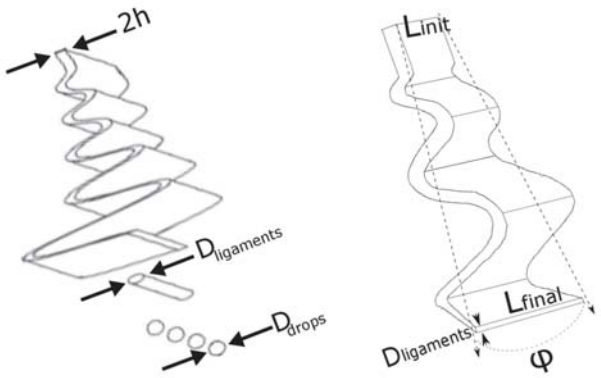

Figure 1 : Left, schematic of the atomisation model for one specific sheet; Right: effect of the sheet stretching

It has to be noted that, at least in this particular case of these nozzles, the result of the primary rupture is to break the circular liquid jet into bidimensional sheets, mostly due to 1) the presence of vapor locations in between the liquid sheets 2) the hydrodynamic in the nozzle that generates an expanding flow at the exit. Therefore the analysis is done on each individual, 2D sheet. Evidence of such sheets will be shown later Figure 1 and 4. Obviously this is a strong modeling assumption, and a limit of the present approach that should be completed for a more universal model and different nozzle types. The break-up of bidimensional sheets to ligaments is based on the instability theory of thin sheet. The growing rate and therefore the final size with $\Lambda = {}^{2\pi}/_{K_s}$ are chosen according to Senecal et al. [4].

$$\omega = -2\nu_l k^2 + \sqrt{4\nu_l{}^2 k^4 + \left({}^{\rho_l}/_{\rho_g}\right) U^2 k^2 - \frac{\sigma k^3}{\rho_l}} \tag{1}$$

and

$$D_{ligaments} = \sqrt{\frac{16h}{\Lambda}} \tag{2}$$

The primary ligaments are then submitted to instabilities, and they are subsequently atomized in drops, using simple model [5]:

$$K_{ligaments} = \frac{1}{D_{ligaments}}\left(0.5 + \frac{3\mu_l}{2\sqrt{\rho_l \sigma D_{ligaments}}}\right)^{-1/2} \tag{3}$$

allowing to derive :

$$D_{drops} = \left(\frac{3\pi D_{ligaments}{}^2}{K_{ligaments}}\right)^{1/3} \tag{4}$$

The initial model of Senecal [4] was initially developed for thin sheets as resulting from swirl atomizer. The validity hypothesa are to have a small ratio of density between gas and liquid, which is the case in gasoline engines where the spray is injected in limited counterpressure and to have a Weber number We > 27/16 which is the case in current high pressure injection. In our cases, h > 2um and U_{rel} > 125m/s, then We > 1.79 > 27/16. The break-up length $L = U_{rel} \cdot \tau$ with the break-up time $\tau = 12/\omega(\Lambda)$ results typically in our cases L~O(mm) ; τ ~ O(5-10us) which looks reasonable based on the data available from the literature.
A specificity of our case is the stretching due to the nozzle exit angle φ (Figure 1 right). Due to the internal flow, as characterised for instance by the hole exit angle, the liquid films are extended radially. Each sheet can be stretched

during the break-up time and so by conservation of the mass, its thickness will then diminish. This effect is quantified using the estimation of the flow stretching along the centre of the ligaments and then reintroduced as a correction parameter in the model. An interesting property of the Senecal model equation (1-2) is that instabilities are independent from the sheet thickness. More details of the practical numerical implementation can be found in ref [1]. The typical steps are illustrated Figure 2. The cross stream slice is extracted at one instant at 500um from the hole from the LES-VOF, where the ligaments are separated. Ligaments thickness is extracted using a distance function from centre to boundary (this last one being associated to an arbitrary iso-level of VOF). Then the coefficients due to the stretching but also due to the breakup into drops, equation (4), are computed (bottom left). This local computation is an improvement of the procedure used in ref [1], where the coefficients were estimated only in an average way. All together, it is easy to return the drop population locally (bottom right), the one that will be reinjected stochastically in the lagrangian simulations. Lagrangian computations cannot be described here into detail but are identical to ref [1]. The mesh is identical when comparing different geometries.

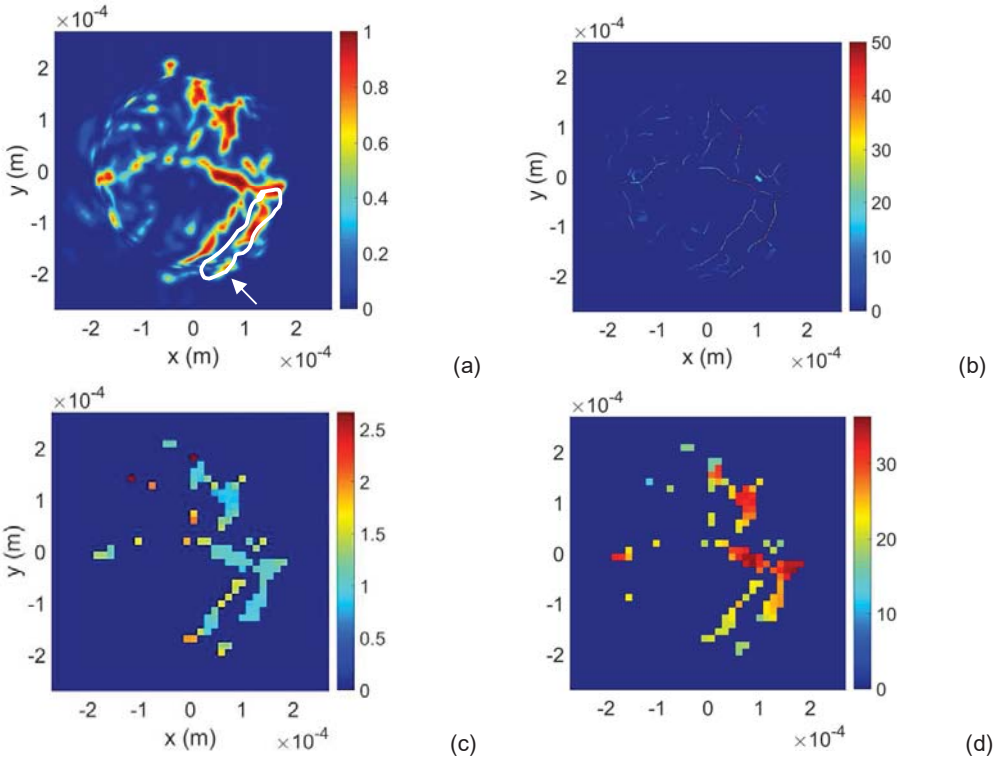

Figure 2 : Ligaments analysis principle on an instantaneous slice. (a) Initial alpha field; (b) distance function at the center of the ligaments; (c) coefficient between ligament and drop size (d) final deduced drop size on this field. The slice is taken perpendicularly to the main direction of the hole. One ligament identification, as modelled fig 1, is indicated on (a), white arrow.

Testcases

The fuel atomizer used here as reference are a special Continental GDI prototype, 3-hole injector (first test, each hole has a different diameter), and 6-hole injector (second test, each hole is inclined differently). The first testcase (Table 1) has holes that are 7% convergent, their length is 345micron, the needle lift is 75um. The second testcase (Table 2) has a needle lift of 100um, with different geometries, extracted from the remeasured ones. The hexahedral mesh is around 15 Mo cells for each case. Each hole is followed by a conical external domain that is meshed up to a length of 5 diameters (Figure **3**). The simulations are two-phase (not 3-phase, which is a limitation of the present approach). Experimental (fixed) mass flow rate is imposed at the inlet, pressure at the exit.

Table 1. Frst testcase, periodic 3-hole injectors

IHole #	**b angle [°]**	**L/D**
1	30	1.7
2	30	2.0

3	30	2.5

Table 2. Second testcase, 6-hole injector

Hole #	b angle [°]	L/D
1	20	1.68
2	30	1.76
3	40	1.90
4	40	1.90
5	30	1.76
6	20	1.68

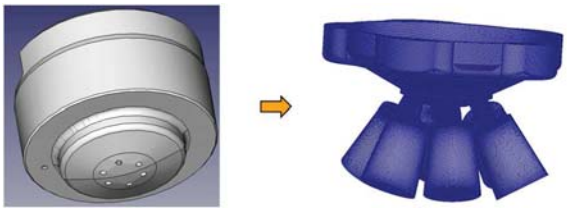

Figure 3 : Left : nozzle CAD ; Right: generated mesh. The 6 cylinders on the bottom represents the external domain (after the nozzle exit) where the atomization process occurs.

Results and discussion, first testcase

The atomization process that has been mentioned above is clearly illustrated Figure **4** for the first testcase. Slices perpendicular to the hole direction are showed in the second part of the hole and in the first part of the atomisation process. The flow development in the hole and at the exit clearly exhibits the breakup into ligaments mostly due to 1) a huge presence of cavitation 2) the ligaments are separated thanks to the radial velocity at the hole exit (as visualised experimentally with the close spray angle at hole exit for instance). A limited hole-to-hole interaction inside the sac volume has been found, due to the high distance between the holes, as only 3-hole are implemented in this prototype test injector. Whatever the hole, shear cavitation is developing largely and reaches the hole exit, even if a small convergence of the hole geometry is present. For holes with the higher diameters, vortex cavitation also develops. Hydraulic flip appears while D is increased. Increasing the hole diameter the primary atomization length is increasing.

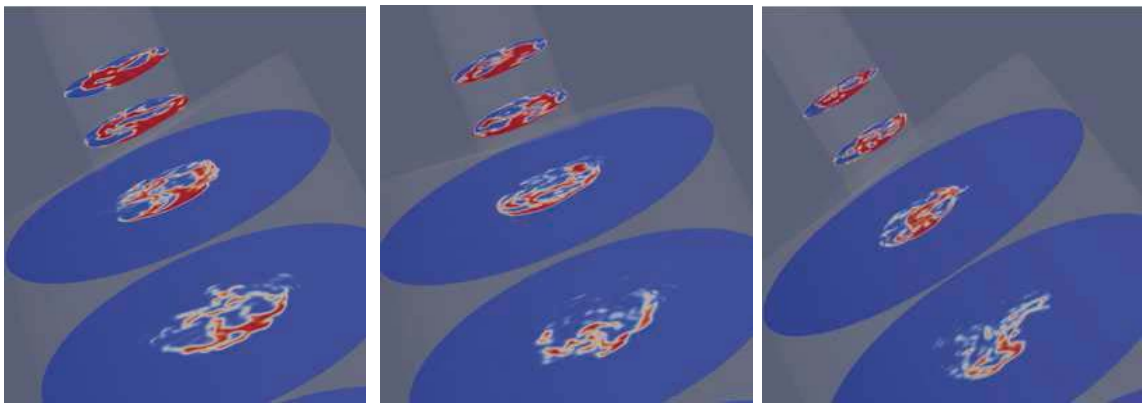

Figure 4 : Instantaneous snapshot of the Volume of Fluid (liquid: red color), 200bar fuel pressure.
Left: large hole diameter ; center: medium hole diameter ; right : small hole diameter. The slices are placed at the hole middle, hole exit, one and two diameters distance after the hole exit (hole length is 345micron)

In the first application case, each hole has a different diameter. This characteristic is visible in the development of the plumes, computed separately here, Figure 5. The spray from the first hole is much larger than the one from the last, small, hole. The Q-criterion as an indicator of the centers of the vortices classically defined by $\tilde{Q} \equiv \frac{1}{2}\left(\tilde{S}_{ij}\tilde{S}_{ij} - \widetilde{\Omega}_{ij}\widetilde{\Omega}_{ij}\right)$, where $\tilde{S}_{ij}$ is the strain-rate tensor and $\widetilde{\Omega}_{ij}$ is the rotation-rate tensor $\widetilde{\Omega}_{ij} = \left(\partial\tilde{u}_i/\partial x_j - \partial\tilde{u}_j/\partial x_i\right)$, displays, in both cases, roll-up structures close to the injection location which then evolve in helicoïdal structures [1]. In the spray from the small hole, this transition to turbulence is longer: indeed, the spray is denser and its exchange with the entrained gas is expected to be reduced.

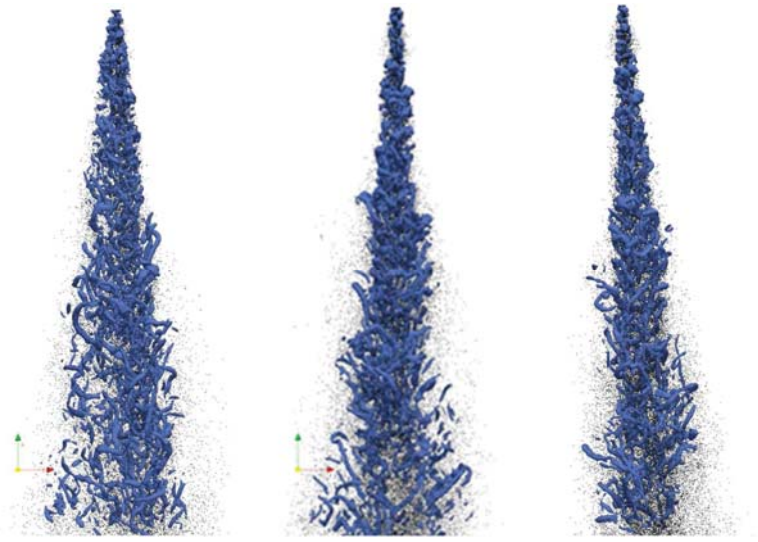

Figure 5 : Instantaneous snapshot of the spray with drop parcels (dots) and isosurface of Q=0.5e9 s^(-1) (blue), 200bar fuel pressure. Left: large hole diameter ; center: medium hole diameter ; right : small hole diameter.

As expected, the studied spray is not sensitive to the smallest scales (τ_p/τ_η > 1 and D_p/η > 1). On the other hand, it is sensitive to the sub-grid scale eddies (τ_p/τ_{sgs} < 1), so a basic sub-grid dispersion model have been introduced in order to take into account this interaction [1]. However, in this dispersion model the main driving factor remains the relative velocity between drops and eddies (τ_{rel}/τ_{sgs} << 1). Fortunately, as the turbulent fluctuations are mostly resolved, $u'/\sqrt{2/3k_{sgs}} \cong 0.95$, the influence of the turbulent dispersion model should remain limited.

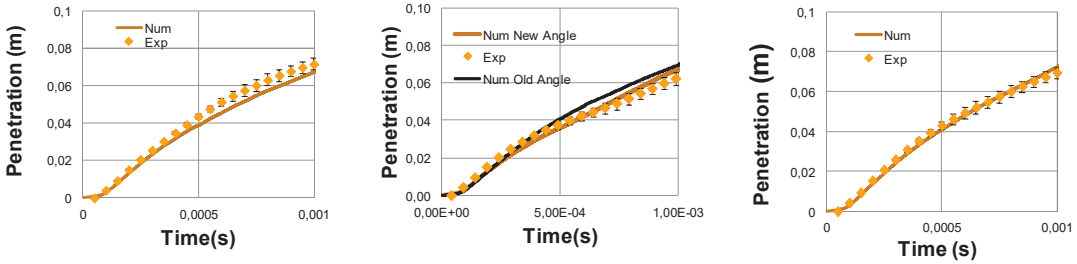

Figure 6 : Penetration curves,) , 200bar fuel pressure.
Left: large hole diameter ; center: medium hole diameter ; right : small hole diameter

To simulate the transient, the single additional input data that is needed is the mass flow rate as a function of time. The specific features at needle opening are initially neglected, using only full lift results, as will be discussed later. Temporal penetration curve in the direction of the spray are compared Figure 6. The global behaviour is satisfactory, slightly lower than the experimental one for the small hole case. Initially, a large difference was found for the medium-diameter hole. Its reason is now explained. Regarding the transient phenomena, in ref [6] the spray exhibited a flapping behaviour at the needle opening, impacting the spray penetration and which had been reproduced successfully in the simulations. In the present testcase, the transient influence of the needle opening is also highlighted. Indeed, with (only) the medium hole of this prototype injector a spurious behaviour was found experimentally: an important increase of the spray angle at the beginning of the injection: the exit angle is increasing

from 25° to 45° during the period 0.1ms-0.4ms. When applying this angle increase in our simulation a satisfactory penetration is recovered back, which was not the case without taking this angle increase into account as the slope change was not captured (figure 6). This result confirms that the transient opening phase has to be measured into detail to be re-introduced empirically as in the present work. Otherwise moving mesh has to be used to simulate the opening needle phase as in ref [3].

Results and discussion, second testcase

Orientation angle B also clearly influences the cavitation behaviour, as seen Figure **8**. Flow detachement is increasing with higher angles, and therefore the shear cavitation (right part of the nozzle slice) is progressively visible. For a small angle, a flow reattachment is visible on both sides, without hydraulic flip, and with a strong presence of cavitation vortex. For an intermediate to large angle, strong shear and vortex cavitation developments generate tridimensional effects and, in average, display a typical “smiley” shape.
In addition, the flow is strongly asymmetric and unsteady due to the hole-to-hole interaction in the nozzle flow development. The arrows refer to the vicinity of the next holes. The top arrow is in the direction of 20deg-hole ; and bottom toward the 40deg-hole. This is a particular effect of this mirror geometry. It is of great interest to look into the vicinity of the holes (along the circumferential direction), see table 2 & fig 3 for the geometry. The 20deg-hole is in between 30deg-hole and 40deg-hole. The other holes have one neighbour with the same hole direction, reinforcing the stability of the flow. Only the intermediate hole direction has neighbour with different hole orientation.

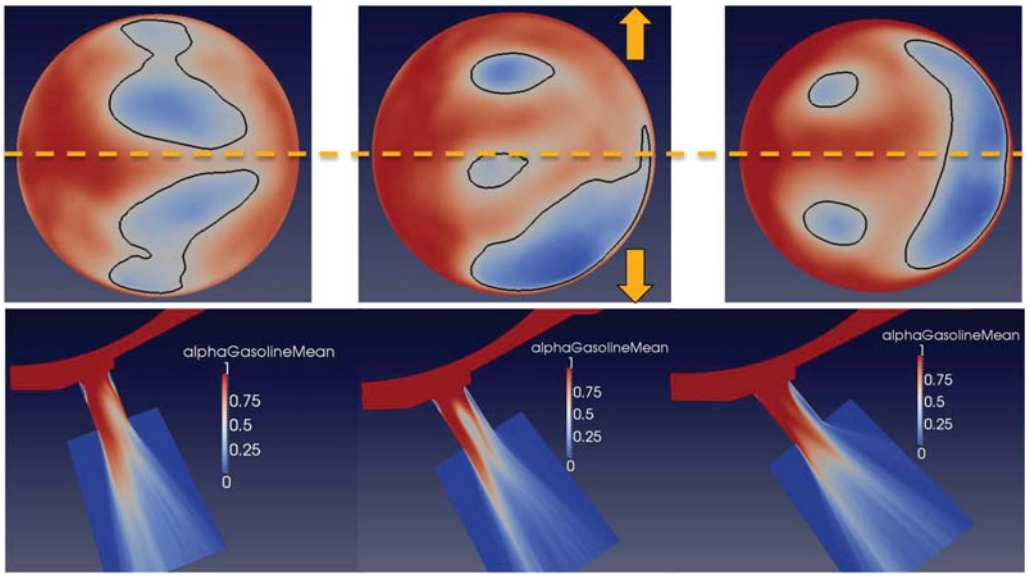

Figure 7 : Time-average of volume of fluid.Red: liquid; blue: vapour. Flow is coming from the right side (needle seat).
Top: Slice at the hole exit, perpendicular to the hole direction axis. Bottom: Cut-plan.
Left: beta angle 20° ; center: beta angle 30° ; right : beta angle 40°
Arrow: see text

The large beta angle shows a stable but reduced cavitating double contrarotating vortices. Stable attached shear cavitation is also present. It leads to a typical “smiley shape” that has been already described with a different injector design but still with a large beta angle of 40deg in ref [1]. Also coherent with this former paper, a side jet appears, due to the reorientation of a liquid sheet in between the two vortices. It can lead to small droplets with high velocity and angle on the side, as has been experimentally confirmed in the former work. Lastly, the higher angles (30deg-40deg) angles exhibit a hydraulic flip. As only two phases (vapour/liquid) are considered here, and not three phases (vapour/air/liquid), we can identify in this simplification a clear limit of the numerical model representation that will be overcome in the future works.
It should be also noticed that the geometry has been generated from a complete 6-holes 3D design, and not from a mirror projected 3 hole case. Therefore, small geometrical differences are intended to be introduced from both sides. However this effect can be lower than in reality, for instance in case of some needle non-axisymetric positioning. This effect can also be damped by the limited resolution mesh. Indeed the flow is found quite stable in

time concerning its pattern, and even comparing the 2 sides. Considering one representative instantaneous flow event, the full picture is provided Figure **8**. Differences are obviously observed, but the number and the area of the cavitating structures are almost identical when comparing both sides, even for 20deg-hole. The captured effect on the average mass flow rate is here not found as the main reason (average mass flow rate differs only by 3%, and instantaneous mass flow rate by less than 10%), but the average flow direction seems to break the symmetry for this 20deg-hole, as already discussed.

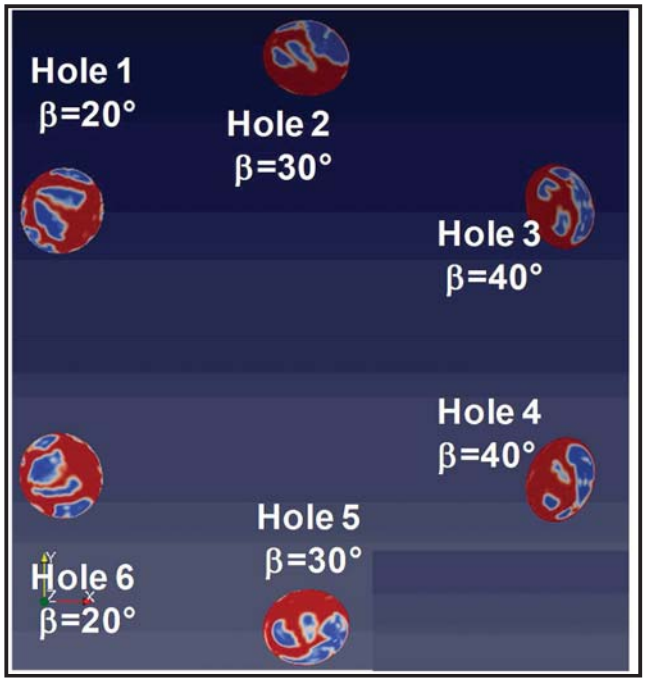

Figure 8 : Instantaneous snapshot of volume of fluid .Red: liquid; blue: vapour.
Cut-plan at the hole exit, projected on a plane perpendicular to the injector central axis.

The spray simulation is now realised with all the plumes injected together. As expected, some jet to jet interaction is observed, especially for the small drops that are entrapped in between the holes. Some turbulent eddies can also connect between the narrowest jets. The general comparison returns a very correct behaviour on Figure 9. The injector is inclined to get the central hole in the vertical direction at the center of the image. The estimation of the external angle depends on the thresholding level that is used, but the tendency is well recovered despite this simple offset.

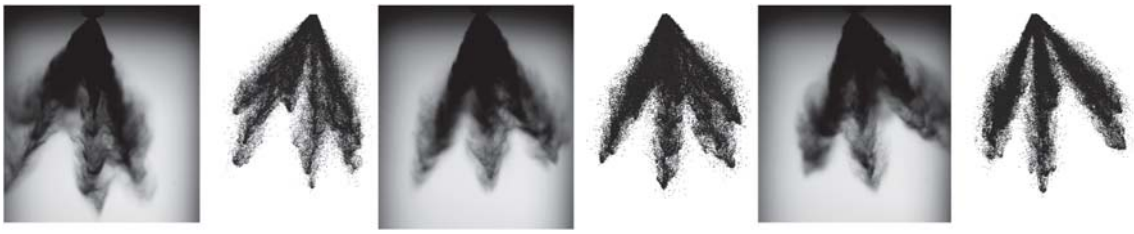

Figure 9 : Instantaneous snaphots of the developed spray a t=1 ms ; experimental shadowgraphy and simulations.
Left: central hole is beta angle 20° ; centre: central hole is beta angle 30° ; right : central hole is beta angle 40°

The experimental penetration is also correctly recovered in Figure 9 and Figure 10, even if the case to case difference is really small, below the RMS shot to shot variation. Interestingly, a manual recording of the typical size of the visible large scale structures of drop segregation returns also a good agreement which explains quantitatively the visible agreement between the images, with fish-bones and drop segregation structures.

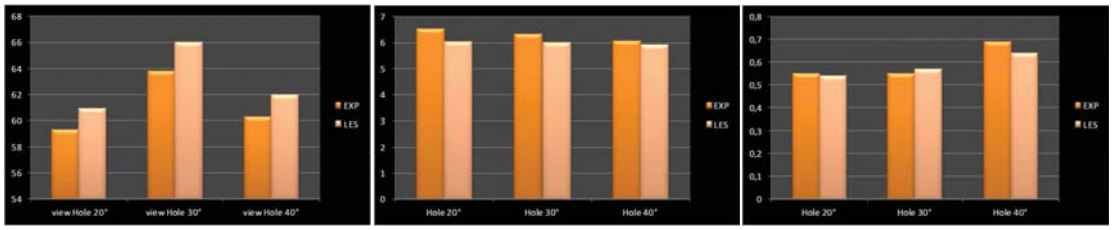

Figure 10 : Resulting comparison of the instantaneous snapshots of the developed spray at 1 ms ; from experimental shadowgraphy and simulations. Top left : total external spray angle; Top right : penetration ; Bottom: large scale structures of drops segregation.

Conclusions

Multijets spray structures, penetrations, and interactions are simulated with large Eddy Simulations. Differences between largely separated holes and narrow holes are depicted, with variations of hole diameters and orientation angles. Comparisons with local quantities will complete this work in the future.

Acknowledgements

CRIHAN and GENCI supercomputer centers are acknowledged for their support. ANR and ANRT are also funding a part of this activity.

Nomenclature

D	Hole diameter [m]
ρ_l	Liquid volumetric mass density [kg/m^3]
ν_l	Liquid viscosity [kg/s.m]
ρ_g	Gas volumetric mass density [kg/m^3]
σ	Surface tension [N/m]
h	Liquid sheet width [m]
τ_p	Drop relaxation time [s]
$D_{ligaments}$	Drop diameter [m]
D_{drops}	Drop diameter [m]
w	Growing rate
k	Wave number [m^-1]
Λ	Maximum unstable wavelength [m]
K	Wave number corresponding to the maximum growth rate
U_{rel}	Relative velocity between the gas and the liquid [m/s]
τ	Break-up time [s]
L	Break-up length [m]
u'	Fluctuating velocity [m/s]
τ_{sgs}	Sub-grid time scale [s]
τ_{rel}	Time for a droplet to traverse an eddy in sub-grid scale [s]
τ_η	Kolmogorov time-scale [s]
η	Kolmogorov length scale [m]
k_{sgs}	Turbulent kinetic energy [m^2/s^2]

References

[1] Helie, J., Khan, M.M., Gorokhovski, M., Journal of turbulence, 2016
[2] Deshpande, S.S., Anumolu, L., Trujillo, MF., Comput Sci Discov. 2012;5:014016.
[3] Piscaglia, F., Montorfano A., Helie J., Demoulin F.-X., International Congress Multiphase Flow, Firenze, Italy, 2016
[4] Senecal, P.K. , Schmidt, D.P., Nouar, I. , Rutland, C.J. , Reitz, R.D., Corradini, M.L., International Journal of Multiphase Flow, vol 25, pp 1073-1097, 1999
[5] Dombrowski, N., and Johns, W.R., Vol. 18, pp. 203-214, Chemical Engineering Science, 1963
[6] J. Hélie, Large Eddy Simulation for Atomization and Spray, LES4ICE, Rueil-Malmaison, 2014